Journal of Process Control 24 (2014) 368–378

Contents lists available at ScienceDirect

Journal of Process Control

journal homepage: www.elsevier.com/locate/jprocont

Closed-loop control of a SCR system using a NO_x sensor cross-sensitive to NH_3

A. Bonfils[a,b,*], Y. Creff[a], O. Lepreux[a], N. Petit[b]

[a] IFP Energies nouvelles, Rond-point de l'échangeur de Solaize, BP 3, 69360 Solaize, France
[b] MINES ParisTech, Centre Automatique et Systèmes, Unité Mathématiques et Systèmes, 60 Bd St-Michel, 75272 Paris, Cedex 06, France

ARTICLE INFO

Article history:
Received 31 December 2012
Received in revised form 25 May 2013
Accepted 18 August 2013
Available online 19 November 2013

Keywords:
Automotive emissions
Diesel engine
NO_x sensor
Selective catalyticreduction
Cross-sensitivity

ABSTRACT

This paper proposes a control strategy for an automotive selective catalytic reduction (SCR) system using a NO_x sensor in a feedback loop. As is representative of real world applications, the employed NO_x sensor is cross-sensitive to NH_3, which induces several complexities. In particular the ambiguity of the measurements could be detrimental to the closed loop response, as it generates multiple equilibrium points (artefacts), besides the point of practical interest. A study of the closed-loop dynamics is performed in the vicinity of each point, which shows that the closed loop system naturally converges to the point of interest not to the artefacts. Experimental results obtained after a detailed calibration method illustrate the relevance and performance of the proposed approach.

1. Introduction

Numerous recent technological developments have yielded substantial improvements in terms of NO_x emissions for diesel engines. These efforts have been so successful that today, reducing NO_x emissions further requires dedicated aftertreatment devices. In theory, among the variety of encountered technologies envisioned for this task (including lean NO_x trap, e.g.), selective catalytic reduction (SCR) is one of the most appealing approach. Unfortunately, the (very) limited measurement possibilities and the complexity of the involved physico-chemical phenomena (reactions and adsorption/desorption effects) are issues making the control of SCR quite challenging. This paper proposes to study the control of such systems, furthering preliminary works appearing in [1].

The SCR systems considered in this paper uses ammonia (NH_3) as the reducing agent to convert NO_x inside a dedicated catalyst. In practice, NH_3 is generated by the decomposition of an urea solution. On the one hand, over-dosing of urea can induce undesired release of NH_3 to the atmosphere (referred to as NH_3-slip) and generate extra-costs for the user. Further, tailpipe NH_3 emissions create unpleasant odors and well-known human health risks. On the other hand, under-dosing results in insufficient NO_x reduction, and possible failure to meet emissions standards. To accurately balance the dosing, control strategies can be used to manage the injection of NH_3.

Recently, several SCR control strategies have been proposed, e.g., [2–5], where it has been proposed to control the amount of NH_3 stored in the catalyst (called NH_3 coverage (ratio) in this paper). For the purpose of applying such methodologies, an NH_3 coverage (ratio) observer based on NO_x sensors measurements must be developed. A particular difficulty is that available embedded NO_x sensors are cross-sensitive to NH_3 [6]. This becomes critical when NH_3-slip is present downstream of the SCR catalyst. Interestingly, the after effects of their use in feedback control strategies have not been much discussed so far. In this paper, this topic is addressed. In the case of a standard observer-controller scheme, the use of the NO_x sensor signal induces problems of observability. Due to the ambiguity between two possible observed states for a given measurement, the observer may become unstable and the after effects on the stability of the closed loop system are unknown. For these reasons, it can be decided to bypass this problem and to consider a way to resolve the ambiguity. The strategy proposed in this paper uses the NO_x sensor measurement to estimate the NH_3 coverage ratio by an output injection state observer. The estimate of the coverage ratio is dynamically forced by the controller to track a setpoint tailored according to current operating conditions. The considered observer-controller consists in a closed loop dynamics coupled to an algebraic equation (defining the stabilizing

* Correspondingauthor at: IFP Energies nouvelles, Rond-point de l'échangeur de Solaize, BP 3, 69360 Solaize, France. Tel.: +33 689907805.
E-mail addresses: anthony.bonfils@ifpen.fr, anthony.bonfils@mines-paristech.fr, anthonybonfils3@gmail.com (A. Bonfils), yann.creff@ifpen.fr (Y. Creff), olivier.lepreux@ifpen.fr (O. Lepreux), nicolas.petit@mines-paristech.fr (N. Petit).

0959-1524/$ – see front matter © 2013 Elsevier Ltd. All rights reserved.
http://dx.doi.org/10.1016/j.jprocont.2013.08.010

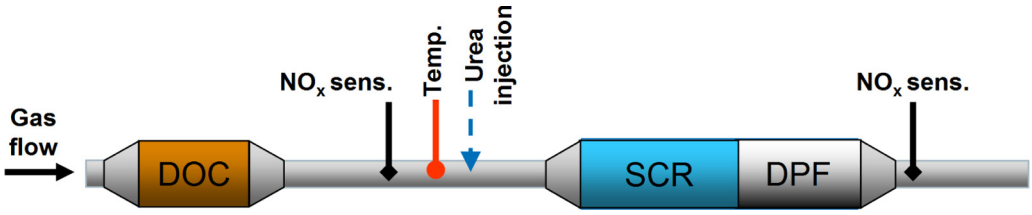

Fig. 1. Exhaust aftertreatment system of the considered experimental setup. Depicted sensors and actuator are used by the control strategy.

controller). Due to the cross-sensitivity of the sensor, this algorithm has several equilibrium points. The list contains the point of practical interest (providing the desired depollution effects) and others. These artefacts could be very troublesome. Study of their stability reveals that the artefacts are either unstable or ambiguity-free. Therefore, the considered control strategy can be tuned to guarantee asymptotic convergence toward the point of practical interest. This is achieved thanks to an additional control mechanism introduced to prevent large NH_3-slip. This paper extends the work previously presented in [1] by explaining in more details the analysis of the closed loop stability. In addition, new experimental results are presented and show the robustness of this strategy.

This paper is organized as follows. First, the SCR operation principle and the related control problem are presented. Then, the system and the sensor models are given, along with a control problem reformulation. Subsequently, a control strategy is proposed. The dynamics of the closed-loop system are studied, which leads to a simple calibration rule. Finally, representative experimental results are presented and report the performances of the considered strategy.

2. SCR system description

2.1. Experimental setup

Fig. 1 illustrates the experimental setup under consideration in this study. The tested exhaust line is composed of a diesel oxidation catalyst (DOC), a SCR catalyst (in this study two different catalysts are used: a Fe-ZSM-5 zeolite and a Cu-ZSM-5 zeolite), and a diesel particulate filter (DPF). A dedicated injection system allows the control of the flow of aqueous urea (AdBlue®). An estimation of the exhaust gas flow rate, the measurements of the inlet temperature sensor and of the two NO_x sensors are available in the control unit, as is pictured in Fig. 1. Moreover, testbench temperatures along the exhaust line, as well as two gas analyzers are available for analysis purposes: a 5-gas analyzer is located upstream of the catalyst and a FTIR analyzer (Fourier Transform InfraRed spectroscopy) downstream of the catalyst.

2.2. SCR catalyst

The SCR catalyst can be viewed as a tubular reactor fed by the exhaust gases coming from the diesel engine. This reactor consists of numerous thin channels which allow the maximization of the transfers to the catalytic surface. Aqueous urea is injected at the reactor inlet. Urea is transformed into NH_3, which is stored (through an adsorption/desorption process) on the active phase of the catalyst [7,8]. The stored NH_3 catalytically reacts with NO_x. From this description, it appears that the NH_3 storage is the key parameter to control NO_x reduction efficiency. The interested reader can refer to [9] for further details. The main chemical reactions are described below.

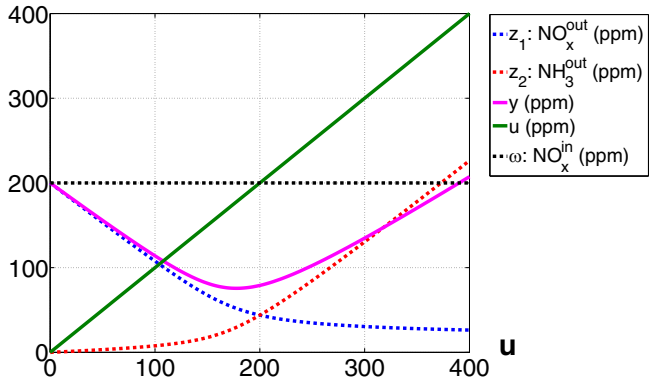

Fig. 2. Outlet NO_x sensor response to increasing NH_3 injection at the inlet of the catalyst (steady state). The temperature, the gas flow rate and the NO_x inlet concentration are respectively set to 300 °C, 100 kg/h and 200 mol ppm.

2.2.1. NH_3 adsorption/desorption

As discussed earlier, the NH_3 in gas phase is adsorbed on the SCR active surface. The adsorbed NH_3 can be desorbed from the substrate. It is represented by the surface coverage ratio, which is the ratio between the number of occupied catalytic sites and the total number of catalytic sites. Adsorption and desorption are complex phenomena that require tedious modeling and calibration efforts. For the most part, they are out of the current scope of our studies.

The direct oxidation of adsorbed NH_3 by oxygen is not presented because it has no impact on the closed-loop analysis. However, adaptation is straightforward.

2.2.2. NO_x reduction

The adsorbed NH_3 reacts with NO_x (and possibly oxygen from the exhaust gas) to produce nitrogen and water [10,11]. In this study, NO and NO_2 are lumped into the total amount of NO_x.

2.2.3. Operating conditions

The system is operated in highly transient conditions. Variations of the exhaust gas flow, the temperature, and the amount of NO_x, respectively, range from 25 to 250 kg/h, 100 to 400 °C, and 10 to 350 mol ppm.

2.3. NO_x sensors and system open loop steady state behavior

The description of the system open loop (stable) static response helps to understand the control issue. In Fig. 2, the steady state values of z_1 (outlet NO_x) and z_2 (outlet NH_3) are represented as a function of u (inlet NH_3 injection), and are compared against the outlet measurement y. It is shown that while u is increased, z_1 decreases (NO_x are reduced) and z_2 increases (NH_3-slip increases). The measurement y delivered by the NO_x sensor located downstream of the catalyst is (with a good level of accuracy) a linear combination of z_1 (NO_x) and z_2 (NH_3) (see [6] for details on the operation principle). As a result, y is non-monotonic: it is close to z_1 when z_2 is small, but largely corrupted when z_2 becomes

significant (i.e. NH_3-slip becomes overwhelming). One can easily appreciate that this behavior can reveal troublesome for feedback control purposes.

As a remark, one shall notice that the inlet NO_x sensor measurement is not polluted by NH_3 since it is located upstream of the injector.

2.4. Problem formulation

A control problem of interest for the SCR system consists of managing the injection of the urea solution in order to maximize the NO_x conversion while maintaining release of NH_3 within acceptable levels (peaks limited to 30 mol ppm, average value less than 10 mol ppm). The system evolves in an environment where the temperature, the gas flow and the amount of NO_x are variable and measured. To achieve the formulated objectives, closed-loop control based on NO_x sensor feedback can be employed. However, as will appear, the NH_3 cross-sensitivity of the NO_x sensor limits the performance of such a control strategy.

3. Input-output description

3.1. Initial model under consideration

Several works [2,12,13] consider a model obtained by material balances for two species with three states: NH_3 and NO_x in gas phase, as well as adsorbed NH_3

$$\begin{cases} \dot{x} = k_a z_2(1-x) - k_d x - k_r z_1 x \\ \dot{z_1} = \dfrac{v}{L}(\omega - z_1) - \Omega k_r z_1 x \\ \dot{z_2} = \dfrac{v}{L}(u - z_2) - \Omega k_a z_2(1-x) + \Omega k_d x \end{cases} \tag{1}$$

where x is the NH_3 coverage ratio, z_1 and z_2 are the NO_x and the NH_3 outlet gas concentrations, respectively. The input u is the NH_3 inlet concentration, and ω is a known and bounded disturbance, the NO_x inlet concentration. All these concentrations are expressed in mol/m^3. Respectively, k_d (in s^{-1}) and k_r (in $m^3/mol/s$) are the reaction rate of desorption and NO_x reduction (defined by Arrhenius laws). k_a (in $m^3/mol/s$) is the constant rate of adsorption [10]. L is the length of the catalyst (in m), v is the gas velocity (in m/s), and Ω is the NH_3 storage capacity (in mol/m^3). The temperature considered in the reaction rates expressions is the average temperature of the catalyst modeled by a first order transfer function

$$T = \frac{T_{in}}{1+\tau s} \tag{2}$$

where T_{in} is temperature at the inlet of the SCR catalyst and τ depends on gas velocity.

The NO_x sensor located downstream of the catalyst delivers an information corrupted by the NH_3 outlet concentration. This sensor can be modeled with a good level of confidence as [14]

$$y = z_1 + \alpha z_2 \tag{3}$$

In this study, α is considered to be a constant value equal to 0.8. This simplifying assumption could be changed, provided that a better knowledge/model of the cross-sensitivity is known.

3.2. Model reduction

To start the analysis, a model reduction is performed (for further details, refer to Appendix A). Consider system (1) where each

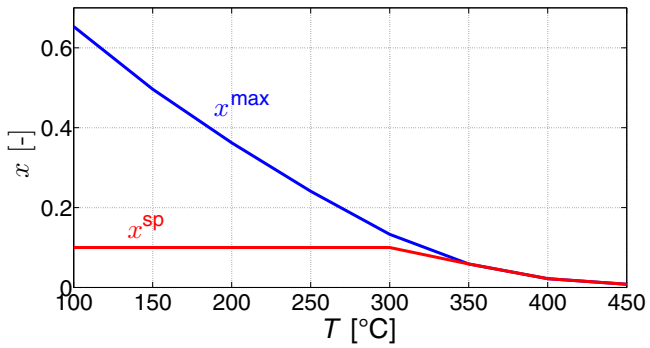

Fig. 3. Maximum coverage ratio with 10 mol ppm of NH_3-slip (x^{max}) and setpoint map (x^{sp}) as functions of temperature.

equation is multiplied by $\epsilon = L/\Omega$ (typically $\epsilon \approx 3.10^{-3}$). In the singular perturbation form [15], one obtains

$$\begin{cases} \dot{x} = f(x, z, u, \omega) & \text{(slow)} \\ \epsilon \dot{z} = g(x, z, u, \omega) & \text{(fast)} \end{cases} \tag{4}$$

where $z = (z_1\ z_2)'$. For any given x, the fast dynamics is asymptotically stable, and $g(x, z, u, \omega) = 0$ has a unique solution

$$z = h(x, \omega, u) = \begin{pmatrix} h_1(x, \omega) \\ h_2(x, u) \end{pmatrix} \tag{5}$$

where

- $h_1(x, \omega) = \frac{\omega}{1+k_r x/\gamma}$;
- $h_2(x, u) = h_{21}(x) + h_{22}(x)u$;
- $h_{21}(x) = \frac{k_d x/\gamma}{1+k_a(1-x)/\gamma}$;
- $h_{22}(x) = \frac{1}{1+k_a(1-x)/\gamma}$;
- $\gamma = \frac{v}{L\Omega}$.

The system (1) can be reduced to its slow dynamics

$$\dot{x} = f(x, h(x, \omega, u), u, \omega) = \gamma(u + h_1(x, \omega) - h_2(x, u) - \omega) \tag{6}$$

This reduction is valid for all positive times because (6) is asymptotically stable.

3.3. Problem reformulation

From the reduction above, one can formulate the SCR control problem with the SISO dynamics (bearing on the coverage ratio)

$$\begin{cases} \dot{x} = \gamma(u + h_1(x, \omega) - h_2(x, u) - \omega) \\ y = h_1(x, \omega) + \alpha h_2(x, u) \end{cases} \tag{7}$$

Because x is not directly measured, a natural idea is to design an observer to provide an estimation $\hat{x}$ and to try to control it to the setpoint x^{sp}.

First, let us explain how x^{sp} can be determined. Maintaining large values of x allows to reach high levels of NO_x reduction efficiency, but increases the NH_3-slip. For this purpose, values of x implying 10 mol ppm of NH_3-slip at steady state are computed as solutions of system (1). It consists, for each operating condition (ω, T and v fixed), to find the steady state input u and therefore the coverage ratio x implying 10 mol ppm of NH_3-slip at steady state. In Fig. 3, these values (denoted x^{max}) are reported as a function of the temperature only, as it plays the most significant role among the parameters. Clearly, x^{sp} should not be chosen greater than x^{max}. Moreover, to prevent possible large NH_3-slip during temperature transients, x^{sp} is further limited by a much lower value (typically 0.1) for low temperatures (with very slight detrimental impact on

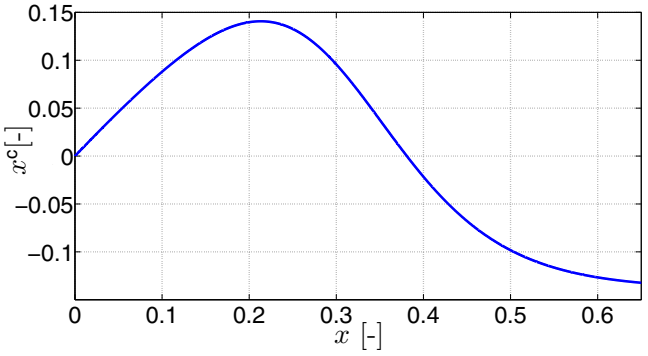

Fig. 4. Interpreted coverage x^c as a function of x (taken at equilibrium), for $T = 250\,^\circ$C, $\omega = 200$ mol ppm, $v = 4.5$ m/s and $x^{sp} = 0.1$.

the efficiency). This limit corresponds to the possibility for the setpoint to be tracked during a fast rise in temperature. Indeed, x can be only decreased slowly at constant temperature (by ω, see (7) with u saturated to 0), while rises in temperature imply vast decreases of x^{max} (see Fig. 3).

The proposed observer is defined, following an output-injection design, as

$$\dot{\hat{x}} = \ell(u, y(x,\omega,u), \hat{x}, \omega) \triangleq \gamma(u + h_1(x,\omega) + \alpha h_2(x,u) - \omega) - k_L(\hat{x} - x^c) \tag{8}$$

where k_L is the observer gain. Implicitly, in this observer design derived from (7), h_2 is neglected because the NH_3-slip is neglected (in theory the choice of x^{sp} leads to low levels of NH_3 at the outlet of the catalyst) and h_1 is directly replaced by the measurement y. In (8), y is used to calculate a tentative value x^c of the coverage, as

$$x^c = h_1^{-1}(y,\omega), \text{ i.e. } \quad h_1(x^c,\omega) = y \tag{9}$$

As y is not invertible with respect to x, it must be noted that only the (dominant) part h_1 is inverted in (9) (NH_3-slip is neglected due to the choice of x^{sp}) and x^c is calculated with the two NO_x sensors signals. This strong simplification yields the mapping represented in Fig. 4 (for low values of x, x^{sp} is close to x).

In this figure, for most of the values of the interpreted coverage x^c, the true coverage x can take two distinct values. Out of those two, the desired one is always the smallest. The real control design problem is to know, for a given x^c, which value of x has to be considered in the feedback strategy. The control law proposed in the next section addresses this issue.

4. Control strategy

In this section, the control strategy is introduced, and an analysis of the closed-loop dynamics is performed.

4.1. Proposed control strategy

The control strategy is designed to force $\dot{\hat{x}} = -k_P\left(\hat{x} - x^{sp}\right)$. The linearizing feedback law is saturated for negative values to account for the actuator limitations. This yields

$$\xi(y(x,\omega,u),\hat{x},\omega,u) \triangleq u - \max\left(0, \omega - y + \frac{1}{\gamma}\left[k_L\left(\hat{x} - x^c\right) - k_P\left(\hat{x} - x^{sp}\right)\right]\right) = 0 \tag{10}$$

The closed-loop system consisting of (7)–(10) is

$$\begin{cases} \dot{x} = f(x, h(x,\omega,u), u, \omega) \\ \dot{\hat{x}} = \ell(u, y(x,\omega,u), \hat{x}, \omega) \\ 0 = \xi(y(x,\omega,u), \hat{x}, \omega, u) \end{cases} \tag{11}$$

4.2. Description of closed loop equilibria

The analysis of closed loop equilibria needs to consider the case of saturated control $u = 0$, which leads to the only equilibrium point of practical interest $(0\ 0)'$ (for further details refer to Appendix B.1). The case of unsaturated control always satisfies $\hat{x} = x^{sp}$ (obtained by substituting the unsaturated control $\Phi(.)$ defined in (15) into the observer equation $\ell(.)$) and the existence of an equilibrium curve of x as a function of k_L. The nature of these curves depends on the value of several parameters (see Figs. 7–9). The stability analysis is more involved.

Generally, the system has one or three equilibrium points, which solely depend on the value of k_L. Indeed, for a given $x \in [0, 1]$,

$$0 = f(x, h(x,\omega,u), u, \omega)$$

is solved, that gives

$$0 = \gamma(u + h_1(x,\omega) - h_2(x,u) - \omega)$$

and

$$0 = u + h_1(x,\omega) - h_{21}(x) - h_{22}(x)u - \omega$$

or, equivalently

$$u(1 - h_{22}(x)) = \omega + h_{21}(x) - h_1(x,\omega)$$

Then, one obtains, $\forall x \in [0, 1]$,

$$u = \frac{\omega + h_{21}(x) - h_1(x,\omega)}{1 - h_{22}(x)} \tag{12}$$

with $1 - h_{22}(x) > 0$ and $\omega - h_1(x) \geq 0$ which gives $u \geq 0$.

Then, the expression of k_L as a function of x is determined by replacing $u(x)$ from (12) into $\ell(u, y(x,\omega,u), \hat{x}, \omega) = 0$. Eventually, one obtains the condition

$$k_L = \gamma \frac{u(x)(1 + \alpha h_{22}(x)) - \omega + h_1(x,\omega) + \alpha h_{21}(x)}{x^{sp} - x^c(x)} \tag{13}$$

Remark 1. For a given x, there exists at most one k_L.

Remark 2. It is needed to consider only positive k_L due to the instability of all the equilibrium points close to the setpoint obtained by a negative k_L.

On the domain of interest for the variables ω, x^{sp}, T, v, the system presents a bifurcation when the parameter k_L is varied. In Fig. 5a, the equilibria are represented for different k_L (derived from (13)), $T = 250\,^\circ$C, $\omega = 200$ mol ppm, $v = 4.5$ m/s and $x^{sp} = 0.1$. The stable equilibrium points are depicted in black and the unstable one in red. In Fig. 5b, the eigenvalue λ_1 (defined in (16)) is represented as a function of x. Then, a zoom on x axis of Fig. 5 is depicted in Fig. 6. Finally, Fig. 7 is obtained from Fig. 5a by choosing a positive gain k_L. Note that the expression of k_L may be not defined for all $x \in [0, 1]$. Indeed, $x^{sp} - x^c = 0$ is a polynomial function of order 2 ($ax^2 + bx + c = 0$), where

$$\begin{cases} a = -k_r^2 x^{sp} k_d - \gamma\omega k_r k_a - \gamma k_d k_r \\ b = -k_r x^{sp}\gamma k_d + k_r x^{sp}\gamma\omega k_a - k_r^2 x^{sp}\gamma\omega + \gamma\omega k_r k_a \\ \quad -\gamma^2 k_d - \gamma^2\omega k_r \\ c = -k_r x^{sp}\omega\gamma k_a \end{cases} \tag{14}$$

Depending on the operating conditions (especially T and ω), the discriminant may be positive (then x can take two distinct values, denoted x_1^* and x_2^*, see Fig. 6) or negative (no real solution for x, see Figs. 8 and 9).

Stability is studied using the Jacobian of the closed loop dynamics, obtained through the implicit function theorem applied to the

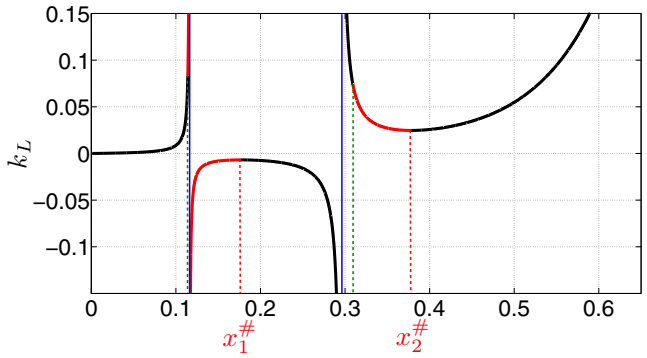

(a) Equilibria of the closed loop dynamics.

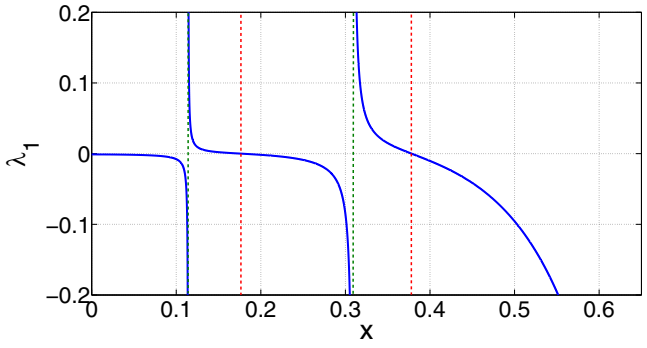

(b) Eigenvalue λ_1.

Fig. 5. Equilibriaof the closed loop dynamics (11) and the eigenvalue λ_1 as functions of k_L. The stable equilibrium points are represented in black and the unstable ones in red. (a) Equilibria of the closed loop dynamics and (b) Eigenvalue λ_1. (For interpretation of the references to color in this figure legend, the reader is referred to the web version of the article.)

algebraic equation u (which is assumed to be not saturated):

$$\Phi(y(x,\omega,u),\hat{x},\omega,u) \triangleq u-\omega+y - \frac{1}{\gamma}\left[k_L\left(\hat{x}-x^c\right)-k_P\left(\hat{x}-x^{sp}\right)\right]=0 \quad (15)$$

In general, the two eigenvalues along the x axis and $\hat{x}$ axis (λ_1 and λ_2, respectively) are defined as follows

$$\begin{cases}\lambda_1 = \dfrac{\partial f}{\partial x}-\dfrac{\partial f}{\partial u}\left(\dfrac{\partial \Phi}{\partial u}\right)^{-1}\dfrac{\partial \Phi}{\partial x}\\ \lambda_2 = -k_P\end{cases} \quad (16)$$

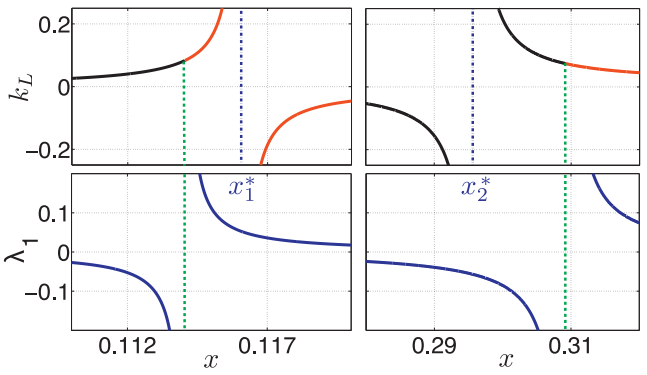

Fig. 6. Equilibria of the closed loop dynamics (11) and the eigenvalue λ_1 as functions of k_L. Zoom on x axis, close to the singularities of λ_1.

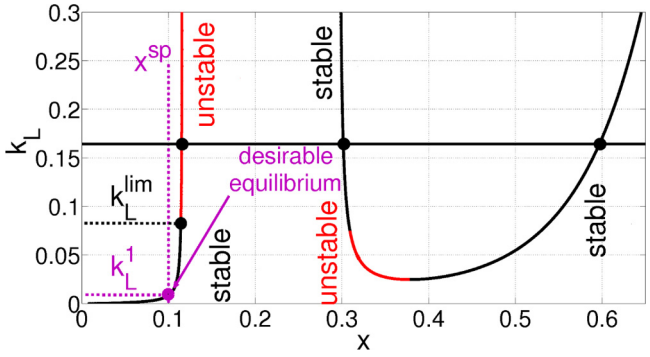

Fig. 7. Equilibria of the closed loop dynamics (11) as function of k_L ($T=250\,^\circ$C, $\omega=200$ mol ppm, $v=4.5$ m/s and $x^{sp}=0.1$). The stable equilibrium points are represented in black and the unstable ones in red. (For interpretation of the references to color in this figure legend, the reader is referred to the web version of the article.)

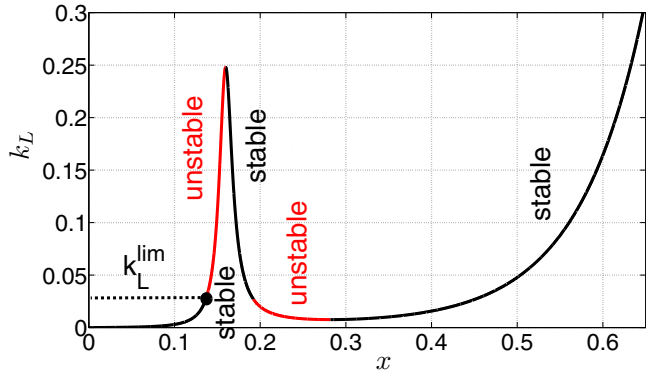

Fig. 8. Equilibria of the closed loop dynamics (11) as function of k_L ($T=250\,^\circ$C, $\omega=70$ mol ppm, $v=4.5$ m/s and $x^{sp}=0.1$). The stable equilibrium points are represented in black and the unstable ones in red. (For interpretation of the references to color in this figure legend, the reader is referred to the web version of the article.)

The first eigenvalue λ_1 is a discontinuous function. Its sign changes on two separate occasions (see Figs. 5b and 6): around the singularities (values of x such that $(\partial\Phi/\partial u)=0$) and when $(\partial k_L/\partial x)=0$ (values of x denoted $x_1^\#$ and $x_2^\#$ in Fig. 5a). Indeed, the condition $\lambda_1=0$ is equivalent to $k_L=k_L^\#$ which rewrites $(\partial k_L/\partial x)=0$ (one can refer to Appendix B.2.1 for further details). The second eigenvalue λ_2 is always negative since $k_P>0$ by construction.

As shown in Figs. 7 and 8, for a small k_L, there is only one stable equilibrium point close to the setpoint. This is the desired equilibrium. When k_L is increased, two more points appear. The first equilibrium (desired) is stable, the second one is unstable and the

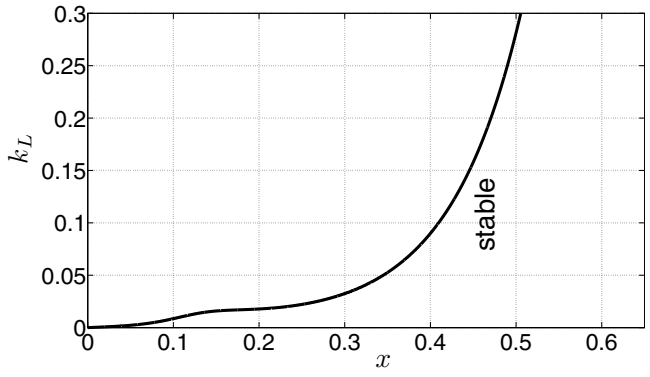

Fig. 9. Equilibria of the closed loop dynamics (11) as function of k_L ($T=250\,^\circ$C, $\omega=20$ mol ppm, $v=4.5$ m/s and $x^{sp}=0.1$).

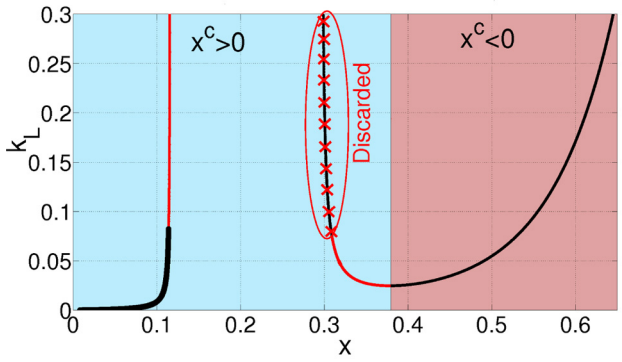

(a) Equilibria of the closed loop dynamics in discrete time.

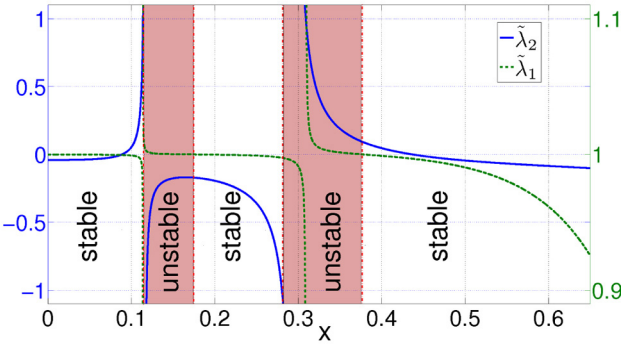

(b) Eigenvalues $\tilde{\lambda}_1$, $\tilde{\lambda}_2$ on x axis and u axis, respectively.

Fig. 10. Equilibria of the closed loop dynamics (11) and eigenvalues in discrete time as functions of k_L. The region where NH_3-slip is detected ($x^c < 0$) is in 10a and the one where it is not detected ($x^c > 0$) in blue. The undesirable points, discarded by the implementation in discrete time (17) of the closed loop dynamics, are represented. (a) Equilibria of the closed loop dynamics in discrete time. (b) Eigenvalues $\tilde{\lambda}_1$, $\tilde{\lambda}_2$ on x axis and u axis, respectively. (For interpretation of the references to color in this figure legend, the reader is referred to the web version of the article.)

last one, which corresponds to a very high coverage, is stable too. Fig. 7 and 8 report the existence of an upper bound for k_L (denoted k_L^{lim}), from which the desired equilibrium point is no longer stable. Slightly below this critical value, the second equilibrium becomes stable. These critical points do not exist in all cases as depicted in Fig. 9; in this case (for a small ω), $\forall x \in [0, 1]$, $(\partial\Phi/\partial u) > 0$.

4.3. NO_x measurement interpretation: detection of NH_3-slip

The closed loop dynamics (11) asymptotically reaches one of the stable equilibria, out of which only the smallest one is of interest, as already discussed. Fortunately, being in the vicinity of the largest-valued undesirable equilibria can be easily detected thanks to the downstream NO_x sensor, without any risk of misinterpretation. Indeed, when $x^c < 0$, the measurement of the inlet sensor is lower than the measurement at the outlet ($x^c < 0 \Leftrightarrow (\gamma/k_r)((\omega/y) - 1) < 0 \Leftrightarrow \omega < y$). In the measurement y, it is clear that the part h_2 is overwhelming the useful signal h_1 (see Fig. 2, when y is greater than ω). With certainty, the sensor measures NH_3. The region of NH_3-slip detection is pictured in Fig. 10a. When this occurs, the following actions are carried out. First, the observer state $\hat{x}$ is set to the maximum coverage ratio before NH_3 desorption of 10 mol ppm. This coverage is taken from the *a priori* x^{max} map presented in Fig. 3. This leads to stops the NH_3 injection and it is kept null as long as $\hat{x}$ is greater than x^{sp}.

4.4. Discarding the remaining undesirable stable equilibrium

The proposed feedback controller is implicit, due to the algebraic equation (10). A possible explicit implementation in discrete time is as follows (Δ_t being the sampling period):

$$\begin{cases} x_{k+1} = x_k + \Delta_t f(x_k, h(x_k, \omega_k, u_k), u_k, \omega_k) \\ \hat{x}_{k+1} = \hat{x}_k + \Delta_t \ell(u_k, y_k(x_k, \omega_k, u_k), \hat{x}_k, \omega_k) \\ u_{k+1} = \max\left(0, \omega_k - h_1(x_k, \omega_k) - \alpha h_2(x_k, u_k) \right. \\ \qquad \left. + \frac{1}{\gamma}\left(k_L\left(\hat{x}_{k+1} - x_k^c\right) - k_P\left(\hat{x}_{k+1} - x_k^{sp}\right)\right)\right) \end{cases} \tag{17}$$

With this implementation, which contains a fixed-point iteration (the relation giving u_{k+1}), the equilibrium points in discrete time always satisfies $\hat{x}_{k+1} = x_k^{sp}$. One can now reduce the system (17) and consider only the two equations x_{k+1} and u_{k+1}. Respectively, the eigenvalues are $\tilde{\lambda}_1 = 1 + \Delta_t\lambda_1$ and $\tilde{\lambda}_2 = 1 - (\partial\Phi/\partial u)$ (refer to Appendix C for further details). The evolution of these two eigenvalues as functions of x is depicted in Fig. 10b. Interestingly, this discrete time dynamics is unstable for every value of the second stable equilibrium. As a result, this troublesome point is discarded by the implementation of the proposed closed loop controller (see Fig. 10). Indeed, as these critical points always satisfies $(\partial\Phi/\partial u) < -2$, the second eigenvalue $\tilde{\lambda}_2$ is always less than -1 (they become unstable). Combined with the previous detection method, this implementation provides convergence to the (only) equilibrium of interest.

4.5. Gain scheduling methodology

Choosing the value for k_L is critical because it defines the value of the reached equilibrium. The most relevant value for this gain would be k_L^1 (see in Fig. 10a) because it corresponds to x^{sp}. But to account for model uncertainty, the gain k_L can be simply scheduled to provide an acceptable level of performance. An off-line study reveals that k_L can be taken as a piecewise affine function of ω, which leads to values that are valid for the ranges defined in Section 2 and induces acceptable bias in the coverage variable x:

$$\begin{cases} k_L = 0, & \omega < 10\,\text{mol ppm} \\ k_L = \omega\beta, & 10 < \omega < 100\,\text{mol ppm} \\ k_L = 100\beta, & \omega > 100\,\text{mol ppm} \end{cases} \tag{18}$$

where β is a calibration parameter inversely proportional to the temperature. It changes from 1 to 1.10^{-2} when T evolves from 200 to 400°C. Experimental results using this calibration are reported and discussed in the next section.

4.6. Robustness analysis

In this section, the robustness of the proposed control strategy to modeling errors is assessed in simulation by dispersing the model parameters k_i, $i \in \{a, d, r\}$ and Ω. This robustness analysis is performed on the Cu-zeolite model but similar results can be obtained for the Fe-zeolite catalyst. Errors are added on the pre-exponential factors k_{i0} and on the activation energies E_i, $i \in \{d, r\}$, of the reaction rates. These variations consist of additive errors (Δ) of ±20% except for the activation energy of desorption (Δ =+20 % and −5%) in accordance with practical considerations.

For this purpose, the controller consisting of (8)–(10) is coupled with a reference SCR model. The NO_x reduction efficiencies and NH_3-slip resulting from the application of modeling errors are reported and compared against the nominal case. All the inputs of

Table 1
NO_x reduction efficiency and NH_3-slip during a NEDC cycle, nominal case and variations with modeling errors.

Parametric variation			Nominal	
			NO_x reduction efficiency (%)	NH_3-slip (peak value) (ppm)
			81	3
Adsorption	k_a	+20%	81	1
		−20%	81	7
Desorption	k_{d0}	+20%	81	5
		−20%	81	2
	E_d	+20%	80	0
		−5%	81	32
NH_3 storage capacity	Ω	+20%	80	0
		−20%	81	21
NO_x reduction	k_{r0}	+20%	82	3
		−20%	79	3
	E_r	+20%	59	3
		−20%	83	3

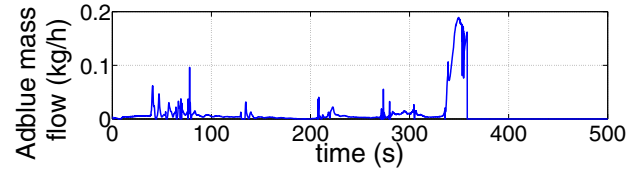

(a) AdBlue® injection.

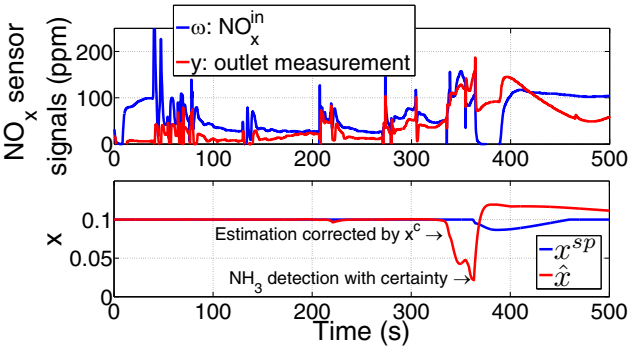

(b) NO_x emissions and coverage ratio evolution.

Fig. 11. Case of a poorly tuned k_L under transient conditions: evolution of the AdBlue® injection, ω, y, x^{sp} and $\hat{x}$ as functions of time. Catalyst: Fe-zeolite. Experimental results. (a) AdBlue® injection and (b) NO_x emissions and coverage ratio evolution.

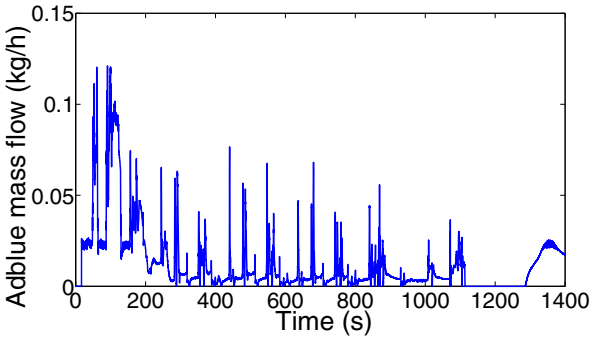

(a) AdBlue® injection.

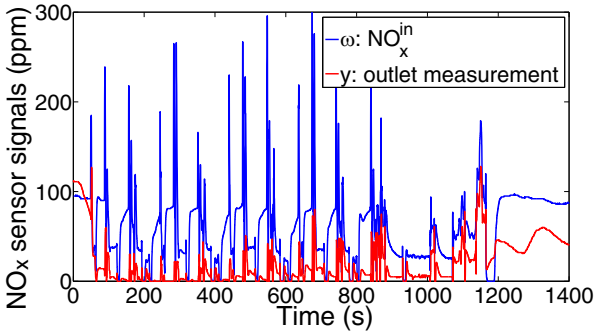

(b) NO_x emissions.

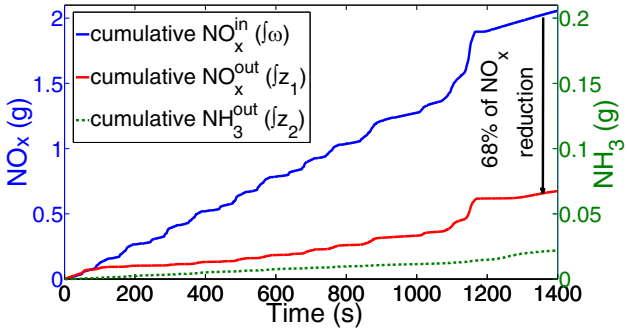

(c) Cumulative NO_x and NH_3 emissions.

Fig. 12. Warm start NEDC cycle with a Fe zeolite catalyst. Experimental results. (a) AdBlue® injection, (b) NO_x emissions and (c) cumulative NO_x and NH_3 emissions.

the model are experimental data obtained by performing a NEDC[1] cycle with warm start on a roller bench. The corresponding experimental results are depicted in Fig. 14 which has been obtained with a Cu-zeolite catalyst. In this cycle, an efficiency of NO_x reduction of 81% is achieved with peak value of NH_3-slip of about 3 mol ppm. The cumulative amount of NO_x at the inlet of the catalyst is 164 mg/km.

Table 1 reports the errors obtained during the simulated cycle.

Note that the two parameters that are the most influent on the amount of outlet NH_3 are the NH_3 storage capacity Ω and the activation energy of desorption E_d. In particular, an underestimation of activation energy of desorption E_d greater than 5% may lead to difficulties in maintaining the release of NH_3 within acceptable levels.

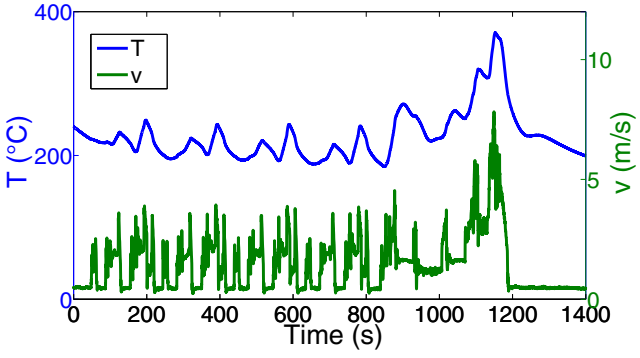

Fig. 13. Variation of temperature and gas velocity during the warm start NEDC cycle. Experimental results.

[1] New European Driving Cycle. This cycle is used in Europe to check the fulfillment of the emission standards.

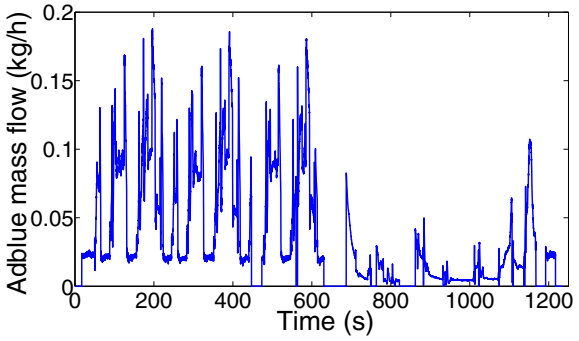

(a) AdBlue® injection.

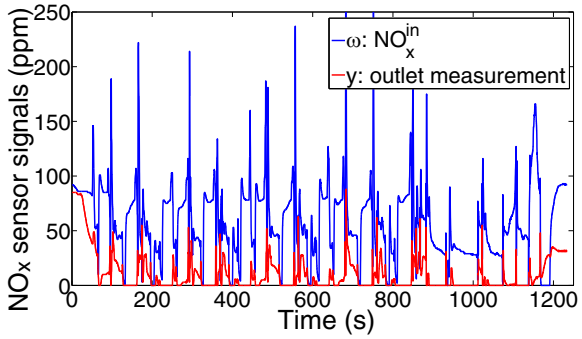

(b) NO_x emissions.

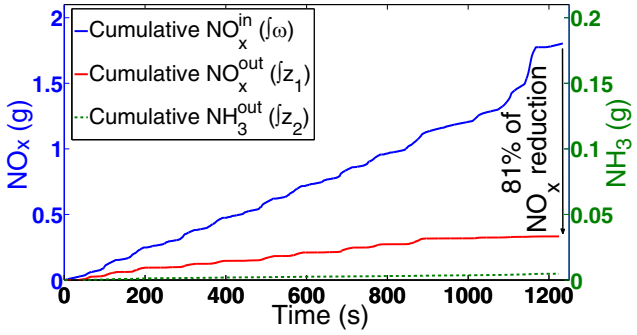

(c) Cumulative NO_x and NH_3 emissions.

Fig. 14. Warm start NEDC cycle with a Cu zeolite catalyst. Experimental results. (a) AdBlue® injection, (b) NO_x emissions and (c) cumulative NO_x and NH_3 emissions.

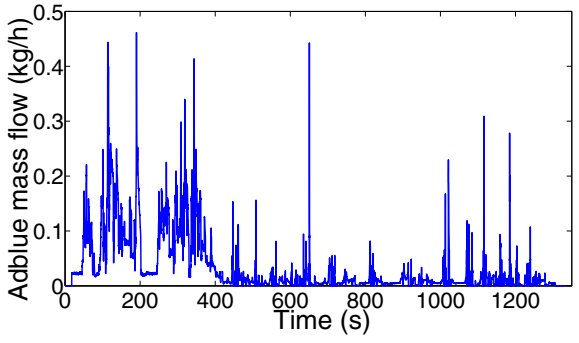

(a) AdBlue® injection.

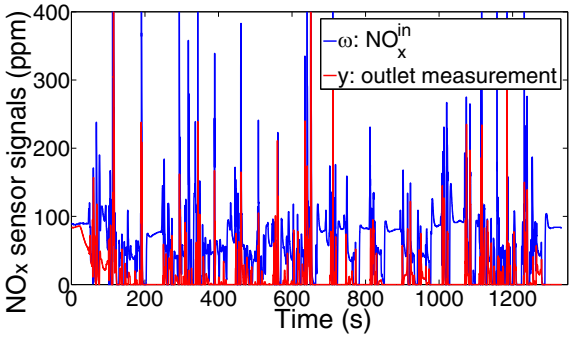

(b) NO_x emissions.

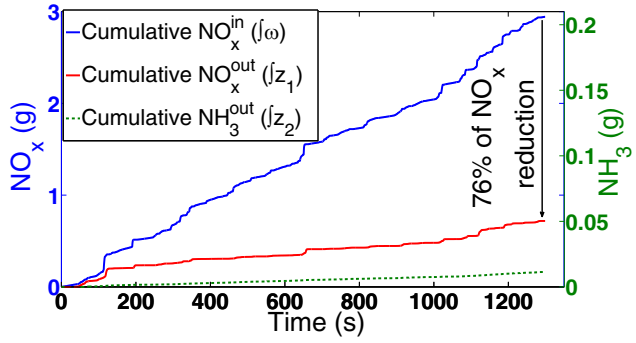

(c) Cumulative NO_x and NH_3 emissions.

Fig. 15. Warm start cycle with a Cu zeolite catalyst. Experimental results. (a) AdBlue® injection, (b) NO_x emissions and (c) cumulative NO_x and NH_3 emissions.

Then, the activation energy of NO_x reduction E_r is an important parameter since an overestimation of 20% of this parameter leads a loss of efficiency of 22%. However, with 59% of NO_x reduction efficiency, the amount of NO_x at the outlet of the catalyst is 68 mg/km, which permits to achieve the Euro 6 standard (80 mg/km).

In conclusion, this study shows that the proposed strategy is fairly robust to modeling errors providing that calibration efforts on the desorption process are made. Furthermore, due to the asymmetric impact of the activation energy of desorption, the robustness of the control law is improved using a conservative calibration of this parameter (E_d is always overestimated).

5. Experimental results

In this section, to illustrate the proposed approach, a fully instrumented vehicle is mounted on a roller test bench and tested under real driving conditions. Two kinds of catalysts are considered to obtain the experimental results (Fe-zeolite and Cu-zeolite).

First, to demonstrate the necessity of scheduling the gain k_L, a test is performed with a poorly tuned k_L. As appears in Fig. 11b, this strategy has relatively limited performance.

Fig. 11b presents the evolution of (ω, y) and $(x^{sp}, \hat{x})$. At about $t = 330$ s, the difference $\hat{x} - x^c$ increases (due to the cross-sensitivity to NH_3, the apparent efficiency calculated from the NO_x sensors decreases): $\hat{x}$ decreases, and u is increased as depicted in the evolution of the AdBlue® mass flow in Fig. 11a. This results in significant NH_3-slip, as can be seen from traces of ω and y. At last, when NH_3 is detected with certainty, the coverage ratio is corrected, and the injection is turned off ($u = 0$). This clearly means that a proper choice of k_L is crucial, as well as a good detection of NH_3-slip is. Then, the proposed gain scheduling method is used and several cycles are performed with the two kinds of catalysts. Model parameters along with control parameters are reported in Table 2. All these tests have been performed with a catalyst which is initially empty at the start of the cycle. First, the results on a NEDC cycle with a warm start and a Fe-zeolite catalyst are presented in Fig. 12 and 13.

Table 2
Model parameters for the two kinds of catalysts (Fe-zeolite and Cu-zeolite).

		Fe-zeolite catalyst	Cu-zeolite catalyst
Adsorption	k_a (m^3/mol/s)	4.1	5.9
Desorption	k_{d0} (s^{-1})	2.67×10^5	4.1×10^5
	E_d (kJ/mol)	85	88.5
NO_x reduction	k_{r0} (m^3/mol/s)	7.19×10^5	2×10^9
	E_r (kJ/mol)	55	82.6
NH_3 storage capacity	Ω (mol^{-3})	70	160
Length	L (in.)	8	9

Fig. 12b and c reports instantaneous and cumulative amounts of NO_x, produced by the engine and released to the atmosphere, respectively. Changes of the temperature and the gas velocity during the cycle are illustrated in Fig. 13. In this test, the control strategy performance is satisfactory, both in terms of NO_x reduction and NH_3-slip limitation. Indeed, the reduction efficiency is about 68% while a very low amount of NH_3 is detected by the FTIR analyzer. NH_3 average concentration is 3 mol ppm over the cycle and 20 mol ppm maximum, which is below usually acceptable limits (average value: 10 mol ppm and maximum value 30 mol ppm).

The curves depicted in Fig. 14b and c have the same meaning than those of Fig. 12b and c, respectively. The performance of the control strategy is quite good too, since a NO_x reduction efficiency of about 81% is obtained with an NH_3 average concentration about 2 mol ppm over the cycle. These good results also show that the proposed strategy can be easily adapted to different types of catalysts.

Finally, another cycle, more transient, with warm start is performed (with a Cu-zeolite catalyst) and the results obtained are depicted in Fig. 15. The performances reached are also highly satisfactory, both in terms of NO_x reduction (76% efficiency) and NH_3 slip limitations (average concentration about 3 mol ppm).

6. Conclusion and future work

In this paper, a control strategy for a selective catalytic reduction (SCR) system has been described. It consists of an observer and a tracking loop. It controls the NH_3 coverage ratio and allows to mitigate the trade-off between NO_x conversion efficiency and tailpipe NH_3-slip. In this strategy, the NH_3 coverage ratio is estimated using the measurement of a commercial NO_x sensor located downstream of the catalyst. This sensor is cross-sensitive to NH_3. It is shown that, in theory, this cross-sensitivity could make the closed-loop system converge to an undesirable value of the coverage ratio as new equilibrium points are created by the feedback loop. The additional and undesirable setpoints are either discarded by the discrete time implementation of the control strategy (which makes them unstable) or detected with certainty from the available data. A parametric study is performed and shows how the observer gain has to be tuned so that the system can remain at all times in the vicinity of the setpoint of interest. As a result, the strategy leads to good performance in most cases, as has been demonstrated on a roller testbench under real transient conditions (several cycles with two different types of catalysts).

Current developments use an observer that reconstructs the (spatially inhomogeneous) profile of the coverage ratio along the catalyst, for an earlier detection of NH_3-slip occurrences. However, one cannot simply apply an output injection with a coverage distribution gradient along the SCR axial direction, a classical observer-controller scheme must be used. Proceeding that way, the problem of observability and misinterpretation of the NO_x sensor signal must be reconsidered.

Appendix A. Model reduction by singular perturbations

Let us consider the system (4) in the singular perturbation form.

A.1. Stability of the fast dynamics

It is easily proved that $\dot{x}$ points inwards on the frontier of [0, 1]. In start for $x=0$ one has $\dot{x} = k_a z_2 \geq 0$; and for $x=1$ one has $\dot{x} = -k_d - k_r z_1 \leq 0$. So for all initial condition $x(0) \in [0, 1]$, $x(t) \in [0, 1]$ for all $t > 0$.

Further, $\forall x \in [0, 1]$, the Jacobian matrix of the fast dynamics is:

$$\frac{\partial g}{\partial z}(x, z, u, \omega) = \begin{pmatrix} -\frac{v}{\Omega} - krxL & 0 \\ 0 & -\frac{v}{\Omega} - ka(1-x)L \end{pmatrix} \tag{A.1}$$

where $x \in [0, 1]$, $\gamma > 0$ and $k_i > 0$, $i \in \{a, r\}$. The eigenvalues of the Jacobian matrix have strictly negative real part, so the fast dynamics is asymptotically stable.

A.2. Fast dynamics equilibria

The condition $g(x, z, u, \omega) = 0$ rewrites as

$$\begin{cases} 0 = \gamma(\omega - z_1) - k_r z_1 x \\ 0 = \gamma(u - z_2) - k_a z_2 (1-x) + k_d x \end{cases} \tag{A.2}$$

or, equivalently

$$\begin{cases} z_1 = h_1(x, \omega) = \dfrac{\omega}{1 + k_r x/\gamma} \\ z_2 = h_2(x, u) = \dfrac{u + k_d x/\gamma}{1 + k_a(1-x)/\gamma} \end{cases} \tag{A.3}$$

where $\gamma = (v/(L\Omega))$

The fast dynamics thus admits a unique solution

$$z = \begin{pmatrix} z_1 \\ z_2 \end{pmatrix} = h(x, u, \omega) = \begin{pmatrix} h_1(x, \omega) \\ h_2(x, u) \end{pmatrix} \tag{A.4}$$

A.3. Reduction to the slow dynamics

The system (4) can be reduced to its slow dynamics (6).

$\forall \bar{x} \in [0, 1]$, equilibrium point of the reduced system, one can solve

$$\left.\frac{\partial f}{\partial x}\right|_{(\bar{x}, \bar{u}, \bar{\omega})} = \gamma \left(-\frac{\bar{\omega} k_r/\gamma}{\left(1 + k_r \bar{x}/\gamma\right)^2} - \frac{1}{\left(1 + k_a\left(1 - \bar{x}\right)/\gamma\right)^2} \left(\left(1 + \frac{k_a}{\gamma}\right) \frac{k_d}{\gamma} + u \frac{k_a}{\gamma} \right) \right)$$
$$< 0, \quad \text{because } k_a > 0, \quad k_d > 0, \quad k_r > 0, \quad \gamma > 0 \quad \text{and} \quad u \geq 0 \tag{A.5}$$

In conclusion, $\forall \bar{x} \in [0, 1]$, $(\partial f/\partial x)|_{(\bar{x}, \bar{u}, \bar{\omega})}$ is always negative. The reduced system is asymptotically stable due to the asymptotic stability of the linearized system around the equilibrium point.

Appendix B. Stability analysis of the closed loop dynamics

B.1. Saturated control $u = 0$

The equilibrium points of system (11) are

$$0 = \frac{\bar{\omega}}{1 + k_r \bar{x}/\gamma} - \frac{k_d \bar{x}/\gamma}{1 + k_a(1 - \bar{x})/\gamma} - \bar{\omega} \tag{B.1}$$

and

$$0 = \gamma \left(\frac{\bar{\omega}}{1 + k_r \bar{x}/\gamma} + \alpha \frac{k_d \bar{x}/\gamma}{1 + k_a(1 - \bar{x})/\gamma} - \bar{\omega} \right) - k_L \left(\hat{\bar{x}} - x^c \right) \tag{B.2}$$

Equivalently (B.2) gives

$$\bar{\hat{x}} = \frac{\gamma}{k_L}\left(\frac{\bar{\omega}}{1+k_r\bar{x}/\gamma} + \alpha\frac{k_d\bar{x}/\gamma}{1+k_a(1-\bar{x})/\gamma} - \bar{\omega}\right) + x^c$$

while (B.1) gives

$$0 = \bar{\omega}\left(1+\frac{k_a(1-\bar{x})}{\gamma}\right) - \frac{k_d\bar{x}}{\gamma}\left(1+\frac{k_r\bar{x}}{\gamma}\right) - \bar{\omega}\left(1+\frac{k_a(1-\bar{x})}{\gamma}\right)\left(1+\frac{k_r\bar{x}}{\gamma}\right)$$

and

$$0 = -\frac{k_d\bar{x}}{\gamma}\left(1+\frac{k_r\bar{x}}{\gamma}\right) - \bar{\omega}\left(1+\frac{k_a(1-\bar{x})}{\gamma}\right)\frac{k_r\bar{x}}{\gamma}$$

then

$$0 = \bar{x}\left[\frac{k_d}{\gamma}\left(1+\frac{k_r\bar{x}}{\gamma}\right) + \bar{\omega}\left(1+\frac{k_a(1-\bar{x})}{\gamma}\right)\frac{k_r}{\gamma}\right]$$

One obtains two distinct solutions for $\bar{x}$. These are detailed below

1 $\bar{x} = 0 \quad \Rightarrow \quad \bar{\hat{x}} = \frac{\gamma}{k_L}(\bar{\omega}+0-\bar{\omega}) + \frac{\gamma(\bar{\omega}-\bar{\omega}-0)}{k_r\bar{\omega}+0} = 0.$

Around this equilibrium point, the triangular form of the Jacobian of the closed loop dynamics has the following eigenvalues: $-k_L < 0$ and

$$\gamma\left(\frac{\partial h_1}{\partial x}\Big|_{(0,\bar{\omega})}(x,\omega) - \frac{\partial h_2}{\partial x}\Big|_{(0,0)}(x,u)\right) = -\omega\frac{k_r}{\gamma} - \frac{1}{(1+k_a/\gamma)^2}\left[\frac{k_d}{\gamma}\left(1+\frac{k_a}{\gamma}\right)\right] \quad < \quad 0$$

In conclusion, the closed loop system is asymptotically stable around $(0 \;\; 0)'$ due to the asymptotic stability of the linearized system.

2 $\bar{x} = \dfrac{-\gamma\left(k_d+\bar{\omega}k_r\left(1+k_a/\gamma\right)\right)}{k_r\left(k_d-\bar{\omega}k_a\right)}$

The case $k_d - \bar{\omega}k_a \geq 0$ which gives $\bar{x} < 0$ corresponds to a non physical solution and must be discarded;

If

$$k_d - \bar{\omega}k_a < 0, \bar{x} = \frac{-\gamma(k_d+\bar{\omega}k_r) - \bar{\omega}k_rk_a}{k_r(k_d-\bar{\omega}k_a)}$$

so

$$\bar{x} = 1 + \frac{-\gamma(k_d+\bar{\omega}k_r) - k_dk_r}{k_r(k_d-\bar{\omega}k_a)}.$$

Consequently, $x > 1$ is also a non physical solution and must be discarded too.

B.2. Unsaturated control

$$u = \omega - y + \left(\frac{1}{\gamma}\right)\left[k_L(\hat{x}-x^c) - k_P(\hat{x}-x^{sp})\right]$$

B.2.1. Proof of the equivalence between $\lambda_1 = 0$ and $(\partial k_L/\partial x = 0)$

The condition $(\partial k_L/\partial x) = 0$ can be rewritten under the equivalent form

$$0 = \left(\frac{\partial u}{\partial x}+\frac{\partial y}{\partial x}\right)\left(x^{sp}-x^c\right) + (u-\omega+y)\frac{\partial x^c}{\partial x}$$
$$0 = \frac{\partial u}{\partial x}+\frac{\partial y}{\partial x}+\frac{k_L}{\gamma}\frac{\partial x^c}{\partial x}$$
$$k_L = -\gamma\frac{(\partial u/\partial x)+(\partial y/\partial x)}{(\partial x^c/\partial x)}$$
$$k_L = \frac{k_r y}{\omega}\left(1+\frac{(\partial u/\partial x)}{(\partial y/\partial x)}\right)$$

and, finally

$$k_L = \frac{k_r y^2}{\omega}\left(1+\frac{(\partial h_1/\partial x)-(\partial h_{21}/\partial x)-(\partial h_{22}/\partial x)u}{(h_{22}(1+\alpha)-1)(\partial h_1/\partial x)-\alpha((\partial h_{21}/\partial x)+(\partial h_{22}/\partial x)u)}\right)$$

This expression is denoted $k_L^{\#}(x)$.

The condition $\lambda_1 = 0$ can be rewritten, equivalently, under the form

$$0 = \frac{\partial f}{\partial x} - \frac{\partial f}{\partial u}\left(\frac{\partial \Phi}{\partial u}\right)^{-1}\frac{\partial \Phi}{\partial x}$$
$$0 = \left(1+\alpha\frac{\partial h_2}{\partial u}+\frac{k_L}{\gamma}\frac{\partial x^c}{\partial u}\right)\frac{\partial f}{\partial x} - \frac{\partial f}{\partial u}\left(\frac{\partial h_1}{\partial x}+\alpha\frac{\partial h_2}{\partial x}+\frac{k_L}{\gamma}\frac{\partial x^c}{\partial x}\right)$$
$$0 = \frac{k_L\omega}{k_ry^2}\left(\frac{\partial y}{\partial u}\frac{\partial f}{\partial x}-\frac{\partial f}{\partial u}\frac{\partial y}{\partial x}\right) - \left(1+\frac{\partial y}{\partial u}\right)\frac{\partial f}{\partial x}+\frac{\partial f}{\partial u}\frac{\partial y}{\partial x}$$
$$k_L = \frac{k_ry^2}{\omega}\frac{(1+(\partial y/\partial u))(\partial f/\partial x)-(\partial f/\partial u)(\partial y/\partial x)}{(\partial y/\partial u)(\partial f/\partial x)-(\partial f/\partial u)(\partial y/\partial x)}$$
$$k_L = \frac{k_ry^2}{\omega}\left(1+\frac{(\partial f/\partial x)}{(\partial y/\partial u)(\partial f/\partial x)-(\partial f/\partial u)(\partial y/\partial x)}\right)$$

and finally

$k_L = \frac{k_ry^2}{\omega}\left(1+\frac{(\partial h_1/\partial x)-(\partial h_{21}/\partial x)-(\partial h_{22}/\partial x)u}{(h_{22}(1+\alpha)-1)(\partial h_1/\partial x)-\alpha\left((\partial h_{21}/\partial x)+(\partial h_{22}/\partial x)u\right)}\right)$ which is precisely $k_L^{\#}(x)$

B.2.2. Solution of $(\partial\Phi/\partial u) = 0$

The condition $\frac{\partial\Phi}{\partial u} = 0$ can be rewritten, equivalently, as

$$0 = 1+\alpha\frac{\partial h_2}{\partial u}+\frac{k_L}{\gamma}\frac{\partial x^c}{\partial u}$$
$$k_L = \frac{k_r\bar{y}^2}{\omega}\left(1+\alpha+\frac{k_a(1-\bar{x})}{\gamma}\right) \tag{B.3}$$

Appendix C. Stability analysis of the discrete time dynamics

One considers the explicit implementation in discrete time described in (17). The corresponding Jacobian matrix is described as follows

$$\begin{pmatrix} J_{11} & J_{12} & J_{13} \\ J_{21} & J_{22} & J_{23} \\ J_{31} & J_{32} & J_{33} \end{pmatrix} \tag{C.1}$$

where

$$\begin{cases} J_{11} = 1 + \Delta_t \dfrac{\partial f}{\partial x} \\ J_{12} = 0 \\ J_{13} = \Delta_t \dfrac{\partial f}{\partial u} \\ J_{21} = \Delta_t \dfrac{\partial \ell}{\partial x} \\ J_{22} = 1 - \Delta_t k_L \\ J_{23} = \Delta_t \dfrac{\partial \ell}{\partial u} \\ J_{31} = -\dfrac{\partial \Phi}{\partial x} + \Delta_t \dfrac{(k_L - k_P)}{\gamma} \dfrac{\partial \ell}{\partial x} \\ J_{32} = \dfrac{(k_L - k_P)}{\gamma} (1 - \Delta_t k_L) \\ J_{33} = 1 - \dfrac{\partial \Phi}{\partial u} + \Delta_t \dfrac{(k_L - k_P)}{\gamma} \dfrac{\partial \ell}{\partial u} \end{cases}$$

The equilibrium points always satisfies $\hat{x}_{k+1} = x_k^{sp}$. Neglecting the effects of the observer convergence, we restrict our analysis to the necessary and sufficient condition for the reduced dynamics having the following matrix governing its discrete-time dynamics.

$$J = \begin{pmatrix} 1 + \epsilon c & \epsilon d \\ -b + \epsilon e & 1 - a + \epsilon f \end{pmatrix} \tag{C.2}$$

where

$$a = \frac{\partial \Phi}{\partial u}, \quad b = \frac{\partial \Phi}{\partial x}, \quad c = \frac{\partial f}{\partial x}, \quad d = \frac{\partial f}{\partial u}, \quad e = \frac{(k_L - k_P)}{\gamma} \frac{\partial \ell}{\partial x},$$

$$f = \frac{(k_L - k_P)}{\gamma} \frac{\partial \ell}{\partial u} \quad \text{and} \quad \epsilon = \Delta_t$$

There exists a change of coordinates to put the previous matrix under triangular form. Thus

$$\det|sI - J| = \begin{vmatrix} s - (1 + \epsilon c - \beta(-b + \epsilon e)) & 0 \\ -(-b + \epsilon e) & s - (1 - a + \epsilon f + \beta(-b + \epsilon e)) \end{vmatrix} \tag{C.3}$$

where β is defined by $\beta^2(-b + \epsilon e) - \beta(a + \epsilon(c - f)) - \epsilon d = 0$

$$\Rightarrow \begin{cases} \beta = a + \epsilon(c - f) \pm \sqrt{\Delta_\beta} \\ \Delta_\beta = a^2 + 2a\epsilon \left(c - f - \dfrac{2bd}{a} \right) + \epsilon^2 \left((c - f)^2 + 4e \right) \\ \qquad = \left(a + \epsilon \left(c - f - \dfrac{2bd}{a} \right) \right)^2 + O(\epsilon^2) \end{cases} \tag{C.4}$$

As a result, the eigenvalues are

$$\begin{cases} \tilde{\lambda}_1 = 1 - \epsilon c - \beta(-b + \epsilon e) \\ \qquad = 1 - a/2 + \epsilon c/2 + \epsilon f/2 + \sqrt{\Delta_\beta} \\ \qquad = \underbrace{1 + \epsilon \left(\dfrac{ca - db}{a} \right)}_{\text{dominant part}} + O(\epsilon^2) \\ \tilde{\lambda}_2 = 1 - a + \epsilon f - \beta(-b + \epsilon e) \\ \qquad = 1 - a/2 + \epsilon c/2 + \epsilon f/2 - \sqrt{\Delta_\beta} \\ \qquad = \underbrace{1 - a}_{\text{dominant part}} + \epsilon \left(\dfrac{fa - db}{a} \right) + O(\epsilon^2) \end{cases} \tag{C.5}$$

In conclusion, for $\Delta_t = \epsilon$ sufficiently small, the following conditions must be satisfied to have asymptotic stability

$$\begin{cases} |1 - a| < 1 \\ ca - db < 0 \end{cases} \tag{C.6}$$

Remark 3.

$$\tilde{\lambda}_1 = 1 + \Delta_t \left(\frac{ca - db}{a} \right) = 1 + \Delta_t \lambda_1.$$

References

[1] A. Bonfils, Y. Creff, O. Lepreux, N. Petit, Closed-loop control of a SCR system using a NO_x sensor cross-sensitive to NH_3, in: Advanced Control of Chemical Processes. 8th IFAC International Symposium, Curran Associates, Inc., 2012, pp. 417–422.

[2] D. Upadhyay, M.J. van Nieuwstadt, Model based analysis and control design of a urea-SCR DeNOx aftertreatment system, Journal of Dynamic Systems, Measurement, and Control 128 (3) (2006) 737–741.

[3] C.M. Schär, C.H. Onder, H.P. Geering, Control of an SCR catalytic converter system for a mobile heavy-duty application, IEEE Transactions on Control Systems Technology 14 (4) (2006) 641–653.

[4] M.F. Hsieh, J. Wang, Backstepping based nonlinear ammonia surface coverage ratio control for diesel engine selective catalytic reduction systems, in: ASME Conference Proceedings, no. 48920, ASME, 2009, pp. 889–896.

[5] M.F. Hsieh, J. Wang, Staircase ammonia coverage ratio profile control for diesel engine two-cell selective catalytic reduction systems, in: Proceedings of the American Control Conference, IEEE, 2010.

[6] R. Moos, A brief overview on automotive exhaust gas sensors based on electroceramics, International Journal of Applied Ceramics Technology 2 (5) (2005) 401–413.

[7] C. Ciardelli, I. Nova, E. Tronconi, B. Konrad, D. Chatterjee, K. Ecke, M. Weibel, SCR-DeNOx for diesel engine exhaust aftertreatment: unsteady-state kinetic study and monolith reactor modeling, Chemical Engineering Science 59 (22-23) (2004) 5301–5309.

[8] L. Olsson, H. Sjövall, R.J. Blint, A kinetic model for ammonia selective catalytic reduction over Cu-ZSM-5, Applied Catalysis B: Environmental 81 (3/4) (2008) 203–217.

[9] A. Frobert, Y. Creff, S. Raux, C. Charial, A. Audouin, SCR for passenger car: the ammonia-storage issue on a Fe-ZSM-5 catalyst, in: SAE International, no. 2009-01-1929, SAE International, 2009.

[10] A. Grossale, I. Nova, E. Tronconi, Study of a Fe-zeolite-based system as NH_3-SCR catalyst for diesel exhaust aftertreatment, Catalysis Today 136 (1-2) (2008) 18–27.

[11] A. Grossale, I. Nova, E. Tronconi, D. Chatterjee, M. Weibel, The chemistry of the NO/NO_2-NH_3 "fast" SCR reduction over Fe-ZMS-5 investigated by transient reaction analysis, Journal of Catalysis 256 (2) (2008) 312–322.

[12] M. Devarakonda, G. Parker, J.H. Johnson, V. Strots, S. Santhanam, Adequacy of reduced order models for model-based control in a urea-SCR aftertreatment system, in: Proceedings of SAE World Congress, no. 2008-01-0617, SAE International, 2008.

[13] M. Devarakonda, G. Parker, J.H. Johnson, V. Strots, Model based control system design in a urea-SCR aftertreatment system based on NH_3 sensor feedback, International Journal of Automotive Technology 10 (6) (2009) 653–662.

[14] M.F. Hsieh, J. Wang, Development and experimental studies of a control-oriented SCR model for a two-catalyst SCR system, Control Engineering Practice 19 (4) (2011) 409–422.

[15] H.K. Khalil, Nonlinear Systems, vol. 3, third ed., Prentice Hall, New Jesrey, 2012.